

Giant transverse magnetic fluctuations at the edge of re-entrant superconductivity in

UTe₂

Valeska Zambra,¹ Amit Nathwani,^{1,2} Muhammad Nauman,^{1,3} Sylvia K. Lewin,^{4,5} Corey E. Frank,^{4,5} Nicholas P. Butch,^{4,5} Arkady Shekhter,⁶ B. J. Ramshaw,^{7,8} and K. A. Modic^{1,*}

¹*Institute of Science and Technology Austria, 3400 Klosterneuburg, Austria*

²*California Institute of Technology, Pasadena, California 91125, USA*

³*Department of Physics and Astronomy, School of Natural Sciences (SNS),
National University of Sciences and Technology (NUST), Islamabad 44000, Pakistan*

⁴*NIST Center for Neutron Research, National Institute of Standards and Technology, Gaithersburg, MD, USA*

⁵*Department of Physics, Quantum Materials Center,
University of Maryland, College Park, MD, USA*

⁶*Los Alamos National Laboratory, Los Alamos New Mexico 87545, USA*

⁷*Laboratory of Atomic and Solid State Physics, Cornell University, Ithaca, NY 14853, USA*

⁸*Canadian Institute for Advanced Research, Toronto, Ontario, Canada*

UTe₂ exhibits the remarkable phenomenon of re-entrant superconductivity, whereby the zero-resistance state reappears above 40 tesla after being suppressed with a field of around 10 tesla. One potential pairing mechanism, invoked in the related re-entrant superconductors UCoGe and URhGe, involves transverse fluctuations of a ferromagnetic order parameter. However, the requisite ferromagnetic order—present in both UCoGe and URhGe—is absent in UTe₂, and magnetization measurements show no sign of strong fluctuations. Here, we measure the magnetotropic susceptibility of UTe₂ across two field-angle planes. This quantity is sensitive to the magnetic susceptibility in a direction transverse to the applied magnetic field—a quantity that is not accessed in conventional magnetization measurements. We observe a very large decrease in the magnetotropic susceptibility over a broad range of field orientations, indicating a large increase in the transverse magnetic susceptibility. The three superconducting phases of UTe₂, including the high-field re-entrant phase, surround this region of enhanced susceptibility in the field-angle phase diagram. The strongest transverse susceptibility is found near the critical end point of the high-field metamagnetic transition, suggesting that quantum critical fluctuations of a field-induced magnetic order parameter may be responsible for the large transverse susceptibility, and may provide a pairing mechanism for field-induced superconductivity in UTe₂.

* kimberly.modic@ista.ac.at

INTRODUCTION

Understanding the connection between magnetism and superconductivity in UTe_2 is key to determining its superconducting order parameters and pairing mechanisms. A compelling feature of UTe_2 is the re-emergence of superconductivity at high magnetic fields in a “halo” of field angles around the b -axis [6]. This re-emergence is coincident with a metamagnetic transition to a spin-polarized state (see Figure 1a). A remarkable feature of both the re-entrant and spin-polarized phases is that they occur in samples that are too disordered to exhibit zero-field superconductivity [2, 13]. This suggests that the pairing mechanism of the re-entrant superconducting phase may be related to the metamagnetic transition.

A comparison can be made with the uranium-based superconductors UCoGe and URhGe , which also exhibit field re-entrant and field-reinforced superconductivity [7]. Unlike UTe_2 , UCoGe and URhGe host ferromagnetic order that onsets at temperatures above the superconducting T_c [1]. In these compounds, it has been suggested that a magnetic field applied perpendicular to the magnetic easy axis induces transverse fluctuations of the ordered moment that drive spin-triplet pairing [3]. While UTe_2 lacks ferromagnetic order at zero field, the fluctuations may be provided by a field-induced phase. However, such fluctuations have not been observed, calling for further study of the magnetism of UTe_2 in high magnetic fields.

Our study focuses on the field-angle phase diagram of UTe_2 at 4 kelvin, where all superconducting phases are suppressed and where the magnetic response can be studied in isolation. We measure the magnetotropic susceptibility [10, 12], which is sensitive to the magnetic susceptibility in a direction perpendicular to the applied magnetic field. We measure in pulsed magnetic fields up to 60 T, and in a full range of angles spanning both the ac - and bc -planes. We find evidence for transverse magnetic fluctuations in both planes, with particularly large transverse fluctuations in a region of the bc -plane that lies at the edge of all three superconducting phases.

EXPERIMENT

We first describe the experimental geometry and why the magnetotropic susceptibility is sensitive to the transverse magnetic susceptibility. The inset of Figure 1a shows the experimental geometry for a magnetotropic susceptibility measurement [10, 12]. A silicon microcantilever is driven near its fundamental bending mode, defining an axis \mathbf{n} around which the tip of the lever oscillates by a small angle $\delta\theta$. We place the cantilever in an external magnetic field \mathbf{B} and rotate the cantilever in the plane normal to the vector \mathbf{n} . This constrains the field angle θ to always lie in the same plane as the lever oscillation angle $\delta\theta$.

The sample is placed on the tip of the cantilever with one crystallographic axis aligned along the length of the lever and another crystallographic axis aligned along \mathbf{n} . For an orthorhombic crystal like UTe_2 , this places the third axis perpendicular to the surface of the lever (inset of Figure 1a). We perform two sets of rotation experiments: one in the

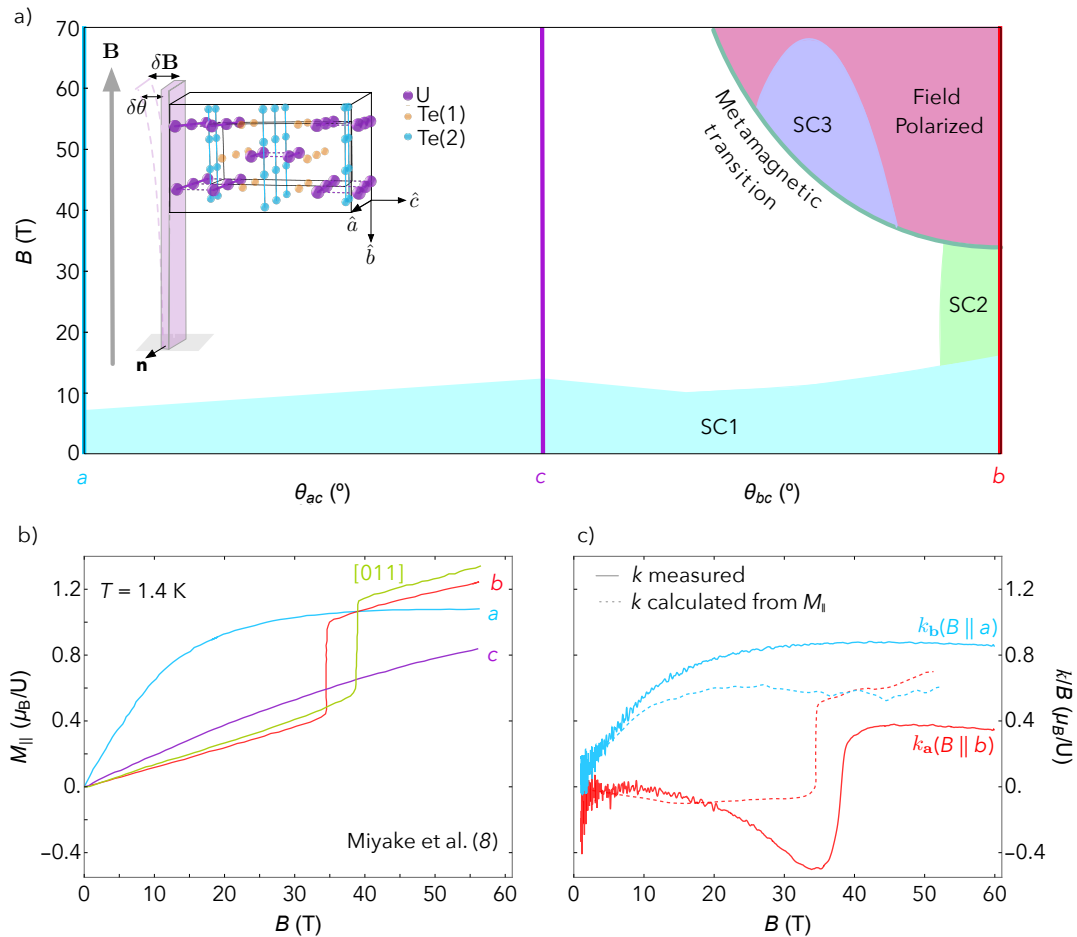


FIG. 1. Phase diagram, magnetization, and magnetotropic susceptibility a) The field-angle phase diagram of UTe_2 at 300 mK, showing the field-angle phase boundaries of the SC1, SC2 and SC3 superconducting states (data reproduced from Helm et al. [4], Knebel et al. [5], and Ran et al. [11]). The colored vertical lines indicate directions where the data in panels b and c were measured. The inset shows the experimental geometry, where \mathbf{B} is the applied magnetic field, and the transverse field component $\delta\mathbf{B}$ results from the vibration of the cantilever by the angle $\delta\theta$ around the axis \mathbf{n} . An example sample orientation is shown for measurements in the bc plane, measuring k_a b) Magnetization as a function of magnetic field applied along each of the crystallographic directions, and in the [011] direction, at $T = 1.4$ K (data reproduced from Miyake et al. [9]). At low field, the a -axis is the magnetic easy axis. At the metamagnetic transition $B_m \approx 35$ T, the magnetization for field along the b -axis jumps to $\sim 1 \mu_B$ per uranium and crosses the a -axis magnetization. c) The magnetotropic susceptibility divided by magnetic field k/B , measured at $T = 4$ K, as a function of field for two different experiment geometries: with the oscillating field component $\delta\mathbf{B}$ in the ac -plane measuring k_b (blue curve), and the oscillating field component $\delta\mathbf{B}$ in the bc -plane measuring k_a (red curve). The subscripts on k denote the normal vector \mathbf{n} to the vibration/rotation plane. The dashed lines are calculated using Equation 1 and the measured magnetization from panel b (e.g. $k_b(\mathbf{B}||b) = B \left(M_b - B \frac{\partial M_c}{\partial B_c} \right)$). The calculated magnetotropic susceptibility captures the overall qualitative behaviour of the measured magnetotropic susceptibility $k_a(B||b)$ and $k_b(B||a)$ —differences may be attributed to the presence of transverse susceptibility components that are not captured in the magnetization measurements.

ac -plane and one in the bc -plane. In all experiments reported here, the c -axis is perpendicular to the surface of the cantilever, and θ is defined as the angle between the applied magnetic field and the c -axis.

When a magnetic field is applied along one of the crystallographic axes of UTe_2 , it produces a magnetic moment parallel to that axis. When the magnetic field is rotated away from that axis, the moment is no longer parallel to the magnetic field. This produces a magnetic torque, $\boldsymbol{\tau} = \mathbf{M} \times \mathbf{B}$, that bends the cantilever by a small angle. The angular

derivative of this torque defines the magnetotropic susceptibility: $k \equiv \partial\tau/\partial\theta$. This susceptibility adds to the elastic bending stiffness of the cantilever and is measured by the shift in the cantilever resonance frequency (see SI for details of the calibration procedure). In terms of the vector \mathbf{n} around which the cantilever oscillates in an applied field \mathbf{B} , the magnetotropic susceptibility is

$$k_{\mathbf{n}}(\mathbf{B}) = (\mathbf{n} \times \mathbf{B}) \cdot (\mathbf{n} \times \mathbf{M}) - \frac{1}{\mu_0} (\mathbf{n} \times \mathbf{B}) \cdot \chi(\mathbf{B}) \cdot (\mathbf{n} \times \mathbf{B}), \quad (1)$$

where $\chi_{ij}(\mathbf{B}) \equiv \mu_0 \partial M_i(\mathbf{B}) / \partial B_j$ is the differential magnetic susceptibility at applied field \mathbf{B} [12]. The first term in Equation 1 captures how the torque changes when a fixed moment \mathbf{M} is rotated in a field \mathbf{B} around the axis \mathbf{n} . The second term captures how the torque changes due to the change in the moment itself as the crystal is rotated in the field.

We can now illustrate why k is sensitive to the *transverse* magnetic susceptibility. The second term of Equation 1 selects the susceptibility tensor component that is perpendicular to both \mathbf{n} and \mathbf{B} . For field along the c -axis, and with the sample oscillating in the ac -plane (bc -plane), this selects $\chi_{aa}(\mathbf{B}||\mathbf{c})$ ($\chi_{bb}(\mathbf{B}||\mathbf{c})$). These are what we define as transverse magnetic susceptibility components. Note that these are *not* off-diagonal susceptibilities, such as $\chi_{bc}(\mathbf{B}||\mathbf{c})$, which are not allowed in an orthorhombic crystal structure for field along crystal axes. Instead, $\chi_{aa}(\mathbf{B}||\mathbf{c})$ and $\chi_{bb}(\mathbf{B}||\mathbf{c})$ are longitudinal (diagonal) susceptibility components that are measured perpendicular to the static, applied magnetic field. The oscillating field component perpendicular to the external field direction is generated by the oscillation of the cantilever (see $\delta\mathbf{B}$ in the inset of Figure 1a). Further experimental details are given the Methods section.

RESULTS

Figure 1c shows the measured magnetotropic susceptibility divided by magnetic field for two different crystal orientations on the cantilever, at 4 K, and with field applied along two different axes: $k_{\mathbf{a}}(\mathbf{B}||\mathbf{b})$ and $k_{\mathbf{b}}(\mathbf{B}||\mathbf{a})$ (see SI for details of the sample orientations). Figure 1b shows the measured magnetization along each of the principal crystallographic directions for comparison (reproduced from Miyake et al. [8]). The metamagnetic transition is clearly visible near 35 tesla for $\mathbf{B}||b$ in both the magnetization and the magnetotropic susceptibility measurements.

The magnetization in Figure 1b is the *longitudinal* magnetization: it is found by integrating the magnetic susceptibility measured *along* the applied field direction, $M_i = \int (\partial M_i / \partial B_i) dB_i$ [8]. We use the longitudinal magnetization and its field derivative—the longitudinal magnetic susceptibility—in conjunction with Equation 1 to calculate the expected magnetotropic susceptibility. This procedure does not account for any nonlinear transverse component to the magnetic susceptibility tensor (these components will be important later). This calculation is shown as dashed lines in Figure 1c for $B||a$ and $B||b$. The overall magnitude and the qualitative features of the calculated and measured magnetotropic susceptibility are in good agreement. Small differences can be attributed to a small misalignment between the rotation vector n , the plane of the cantilever, and the sample's crystal axes. This demonstrates that,

for field along the a - and b -axes, the measured magnetotropic susceptibility is largely determined by the longitudinal magnetic susceptibility. As shown below, this will not be the case for other field orientations.

Figure 2a and b show the magnetotropic susceptibility for magnetic field applied along the c -axis, for both the k_a and k_b configurations. We also reproduce the data and calculations from Figure 1c for comparison. Unlike the other two field orientations, the measured magnetotropic susceptibility for $\mathbf{B}||c$ deviates strongly from the estimate made using the longitudinal magnetization and susceptibility alone (dashed purple line). The large negative response in the magnetotropic susceptibility compared to that inferred from magnetization measurements indicates that a new susceptibility component, hidden from the longitudinal magnetization measurements, becomes active in the magnetotropic susceptibility at a field scale of around 20 tesla.

Panels c and d in Figure 2 show the evolution of the magnetotropic susceptibility for a broad range of field angles in the ac - and bc -planes. The large decrease in the magnetotropic susceptibility that onsets near 20 T for field along the c -axis is observed over a broad range of angles in both planes. In the bc -plane (Figure 2d), the decrease in the magnetotropic susceptibility is abruptly truncated by the metamagnetic transition into the field-polarized phase (red shaded region).

ANALYSIS

We uncover the origin of the large decrease in the magnetotropic susceptibility near 20 tesla by first analyzing the data along a high-symmetry direction. When the magnetic field is applied along a crystal axis, the first term in Equation 1 is completely determined by the longitudinal magnetization. Here, the second term has contributions only from the transverse magnetic susceptibility, i.e. $\chi_{ii}(B||j)$, for $j \neq i$. The longitudinal magnetization, shown in Figure 1b, clearly shows no features that resemble the strong downturn seen in k near 20 tesla. Therefore, the decrease in k for field applied along the c -axis must originate from a transverse component of the magnetic susceptibility, i.e. $\chi_{ii}(B||j)$.

To highlight the large magnitude of the transverse magnetic susceptibility, we convert our magnetotropic data to dimensionless susceptibility units by dividing k by B^2/μ_0 (Figure 3). Next, we subtract out the contributions calculated using the longitudinal magnetization and magnetic susceptibility. The remaining contribution is the transverse magnetic susceptibility. Figure 3 shows this susceptibility for k_a measured with $B||c$, i.e. $\chi_{bb}(B||c)$. We also show the longitudinal susceptibility for the same field orientation, i.e. $\chi_{cc}(B||c)$. By 40 tesla, the transverse magnetic susceptibility is more than $30\times$ larger than the longitudinal susceptibility; quantitatively, the transverse susceptibility is very large in comparison to the longitudinal susceptibility.

Moving away from the c -axis, the large increase in transverse susceptibility persists, and even strengthens, as we move towards the b -axis (Figure 4). Like the longitudinal magnetization measured along the principal axes, the longitudinal magnetization measured at these intermediate angles indicates no substantial changes in the longitudinal

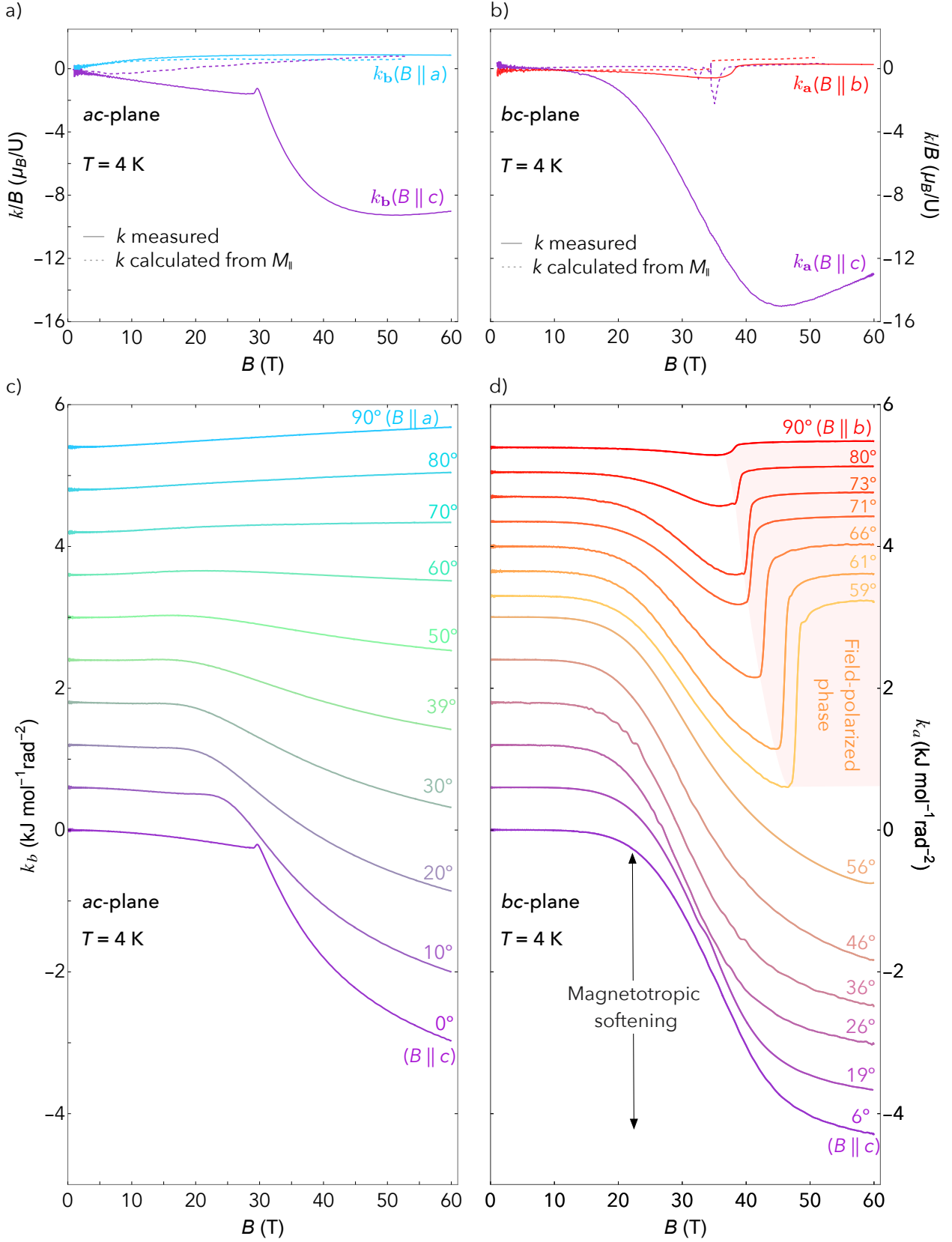


FIG. 2. **Angle-dependent magnetotropic susceptibility.** Magnetotropic susceptibility measurements performed in pulsed magnetic fields up to 60 T. Panel a) shows $k_b(B \parallel c)$ and compares it to $k_b(B \parallel a)$, and likewise for $k_a(B \parallel c)$ and $k_a(B \parallel b)$ in panel b). The dashed lines in both panels are the calculated values of k based on the measured longitudinal magnetic susceptibility data from Figure 1b and Equation 1. Panels c) and d) show the magnetotropic susceptibility measured at multiple angles in the ac - and bc -planes, respectively. As magnetic field approaches the c -axis in both planes, a large decrease is observed in k that onsets at roughly 20 T. This decrease persists for a range of angles in both planes around $B \parallel c$, and is abruptly cut off by the metamagnetic transition into the field-polarized phase (red shaded region in panel d) at $\theta = 59^\circ$ in the bc plane.

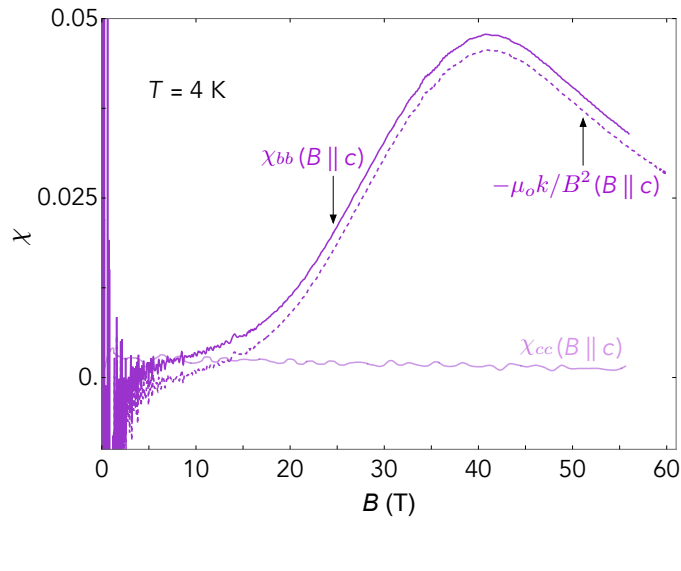


FIG. 3. **Longitudinal and transverse magnetic susceptibility** The dimensionless magnetic susceptibility as a function of magnetic field applied along the c -axis. The light purple curve shows $\chi_{cc} = \mu_o(\partial M_c / \partial B_c)$ obtained from conventional measurements of the longitudinal magnetic susceptibility [9]. The dark purple curve shows the transverse magnetic susceptibility for $B||c$, taken as $\chi_{bb} = \mu_o(\chi_{cc} - k_a/B^2)$.

susceptibility [9]. Therefore, the large decrease in k at all angles must come from an increase in the transverse magnetic susceptibility. While we do not have longitudinal magnetization measurements at all angles, and thus cannot subtract out the longitudinal component at all angles, Figure 3 demonstrates that the transverse component is overwhelmingly larger than the longitudinal component in our measurement and that the transverse susceptibility is essentially equal to $-\mu_0 k/B^2$. We plot this quantity in Figure 4 for angles in the ac and bc planes. The transverse susceptibility is large for a broad region of the bc -plane, and peaks at a field of around 40 tesla and for angles between 10° and 50° away from the c -axis.

DISCUSSION

Figure 4 shows a broad region of large transverse magnetic susceptibility in the ac - and bc -planes of the field-angle phase diagram. As shown in Figure 3, the transverse susceptibility reaches a value more than 30 times larger than the longitudinal susceptibility measured at the same field. A large transverse susceptibility implies large *fluctuations* of the magnetization in the direction transverse to the applied magnetic field, and large magnetic fluctuations are conducive to superconducting pairing.

What could give rise to these large fluctuations? The most natural source would be soft magnons associated with a second-order magnetic phase transition [3]. More specifically, the fact that we observe *transverse* softening indicates that the phase transition is associated with the magnetic moment wanting to re-orient perpendicular to the applied field direction. For example, for $\mathbf{B}||c$, the large transverse susceptibility observed for both crystal orientations indicates that the field-induced moment wants to rotate away from the c axis and into the ab -plane at high fields. The peak

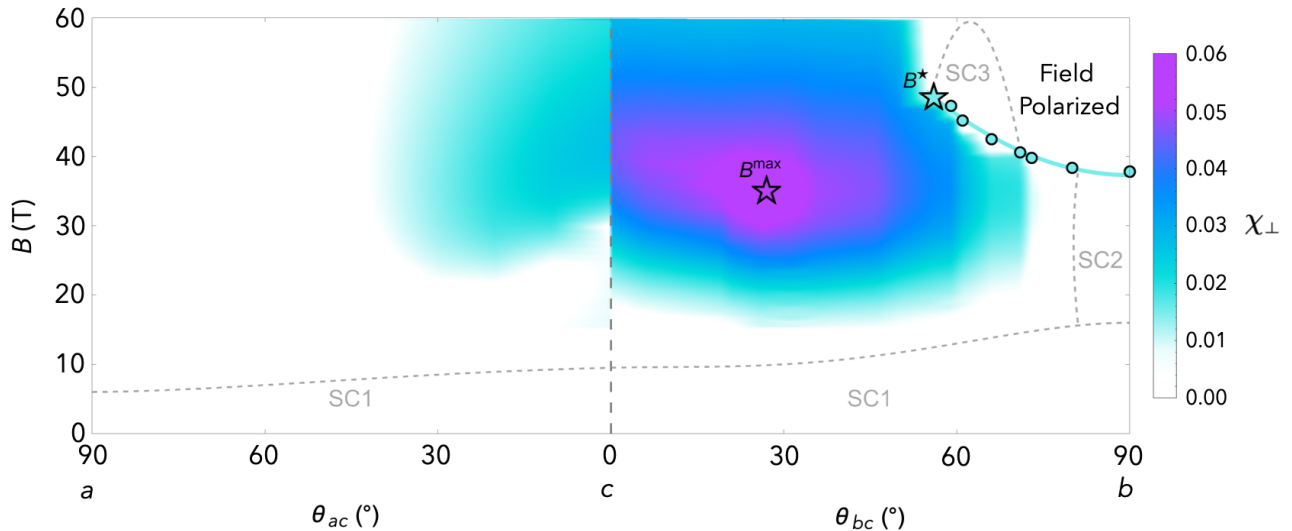


FIG. 4. **Phase diagram of the magnetotropic susceptibility, k_b in the ac -plane and k_a in the bc -plane, divided by B^2 .** A color plot of the magnitude of the magnetotropic susceptibility converted to dimensionless susceptibility units as a function of field strength and field angle in the ac - and bc -plane at 4 kelvin. The measured magnetotropic susceptibility k was multiplied by $-\mu_0/B^2$, which we define as χ_{\perp} . As the longitudinal susceptibility components are not known for all intermediate angles, we cannot subtract those contributions from the measured signal. Rather, we assume, based on Figure 3, that the leading contribution is the transverse magnetic susceptibility. Magenta highlights the angle and field regions where the transverse magnetic susceptibility is largest. The values measured below 15 T are set to zero (white) on this plot because dividing by B^2 makes the noise diverge at low fields. The metamagnetic phase boundary as determined by the jump in k (Figure 2d) is indicated by teal points outlined in black and terminates at the critical endpoint near $\theta = 59^\circ$ as indicated by the teal star. The line through the metamagnetic transition points is a guide to the eye. The phase boundaries for SC1, SC2, and SC3 are taken from Lewin et al. [6] and Knebel et al. [5].

in χ_{\perp} at B^{\max} in Figure 4 indicates the angle and field where the magnetic moment has the maximum tendency to reorientation toward the $\delta\mathbf{B}$ we are probing.

What is the relationship between the large transverse susceptibility and the metamagnetic transition? Figure 2d shows that the jump in the magnetotropic susceptibility across the metamagnetic transition increases in magnitude as magnetic field is rotated toward B^* between 56° and 59° in the bc -plane (teal star in Figure 4). Likewise, Wu et al. [14] have shown that the discontinuity in the magnetization across the metamagnetic transition goes to zero upon approaching B^* . Both of these observations are consistent with B^* marking the second-order critical end point of a line of first-order phase transitions. The fluctuations grow large in the vicinity of the metamagnetic phase boundary, and are abruptly truncated after the moment re-orient in the field polarized phase.

Why are the maximum transverse fluctuations not found right at B^* ? The reason is that our experiment is only sensitive to fluctuations in a direction perpendicular to \mathbf{B} , and the ferromagnetic order parameter does not necessarily grow in this direction at B^* . In other words, there will be divergent magnetic fluctuations for *some* field orientation at B^* , but not in the direction we probe in this experiment. As noted by Wu et al. [14], the critical endpoint at B^* forms a continuous line in field-angle space. Using the phase diagram of Wu et al. [14], we find that the region of maximum transverse susceptibility in our experiment, denoted B^{\max} in Figure 4, is only $\approx 6^\circ$ away from B^* in

another rotation plane. We suggest that at this B^* , the magnetic order parameter grows along the direction $\delta\mathbf{B}$ we probe in our experiment—perpendicular to the applied field at B^{\max} . In the SI, we show data from a second sample oriented in a slightly different plane where we may indeed directly cross B^* in our measurement.

Whatever their origin, strong ferromagnetic fluctuations are expected to be conducive to spin-triplet superconducting pairing [3]. This pairing mechanism was suggested to explain the high-field superconductivity in UCoGe and URhGe [1, 8], which are easy-axis ferromagnets. We find evidence for strong transverse fluctuations over a broad region of the field-angle phase diagram (Figure 4), and we suggest that they may be the “glue” for superconducting pairing in UTe₂.

Measurements of the magnetotropic susceptibility are a new window into the high-field phase diagram of UTe₂. They go beyond traditional measurements of the longitudinal magnetization and susceptibility, and are compatible with pulsed magnetic fields and rotation studies. We reiterate that here we have only measured the transverse fluctuations for one particular sample-cantilever-field-rotation plane configuration. Future experiments will explore both different field-angle planes and different orientations of the \mathbf{n} vector, allowing us to probe different transverse susceptibility components and to determine the exact relationship between ferromagnetic fluctuations and the superconducting phases of UTe₂.

ACKNOWLEDGMENTS

We appreciate technical support from Ali Bangura and Zoltán Köllő.

V.Z., A.N., M.N. and K.A.M. acknowledge support from the European Research Council Starting Grant 101078696-TROPIC. V.Z., A.N., M.N. and K.A.M. thank the ISTA Nanofabrication Facility for technical support. B.J.R. acknowledges funding from the Office of Basic Energy Sciences of the United States Department of Energy under award number DE-SC0020143 for data analysis and writing. The National High Magnetic Field Laboratory is supported by the National Science Foundation through NSF/DMR-2128556*, the State of Florida, and the U.S. Department of Energy. A.S. acknowledges support from the DOE/BES “Science of 100 T” grant. A.S. thanks Downtown Subscription in Santa Fe, NM for their patience in hosting him. Sample preparation and characterization was supported by the NSF through DMR-2105191.

AUTHOR CONTRIBUTIONS

B.J.R. and K.A.M. conceived of the experiment; S.K.L., C.E.F. and N.P.B. prepared and characterized the samples; V.Z., A.N., M.N. and A.S. performed the experiments and analyzed the data. V.Z., B.J.R., and K.A.M. wrote the manuscript with input from all co-authors.

COMPETING INTERESTS

The authors declare no competing interests.

- [1] Dai Aoki, Kenji Ishida, and Jacques Flouquet. Review of U-based Ferromagnetic Superconductors: Comparison between UGe₂, URhGe, and UCoGe. *Journal of the Physical Society of Japan*, 88(2):022001, 2019. ISSN 0031-9015. doi:10.7566/jpsj.88.022001.
- [2] Corey E. Frank, Sylvia K. Lewin, Gicela Saucedo Salas, Peter Czajka, Ian M. Hayes, Hyeok Yoon, Tristin Metz, Johnpierre Paglione, John Singleton, and Nicholas P. Butch. Orphan high field superconductivity in non-superconducting uranium ditelluride. *Nature Communications*, 15(1):3378, 2024. doi:10.1038/s41467-024-47090-1.
- [3] K. Hattori and H. Tsunetsugu. p-wave superconductivity near a transverse saturation field. *Physical Review B*, 87(6):064501, 2013. ISSN 1098-0121. doi:10.1103/physrevb.87.064501.
- [4] Toni Helm, Motoi Kimata, Kenta Sudo, Atsuhiko Miyata, Julia Stirnat, Tobias Förster, Jacob Hornung, Markus König, Ilya Sheikin, Alexandre Pourret, Gerard Lapertot, Dai Aoki, Georg Knebel, Joachim Wosnitza, and Jean-Pascal Brison. Field-induced compensation of magnetic exchange as the possible origin of reentrant superconductivity in UTe₂. *Nature Communications*, 15(1):37, 2024. doi:10.1038/s41467-023-44183-1.
- [5] Georg Knebel, William Knafo, Alexandre Pourret, Qun Niu, Michal Vališka, Daniel Braithwaite, Gérard Lapertot, Marc Nardone, Abdelaziz Zitouni, Sanu Mishra, Ilya Sheikin, Gabriel Seyfarth, Jean Pascal Brison, Dai Aoki, and Jacques Flouquet. Field-Reentrant Superconductivity Close to a Metamagnetic Transition in the Heavy-Fermion Superconductor UTe₂. <https://doi.org/10.7566/JPSJ.88.063707>, 88, 5 2019. doi:10.7566/jpsj.88.063707. URL <https://journals.jps.jp/doi/abs/10.7566/JPSJ.88.063707>.
- [6] Sylvia K Lewin, Peter Czajka, Corey E Frank, Gicela Saucedo Salas, Hyeok Yoon, Yun Suk Eo, Johnpierre Paglione, Andriy H Nevidomskyy, John Singleton, and Nicholas P Butch. High-Field Superconducting Halo in UTe₂. *arXiv*, 2024. doi:10.48550/arxiv.2402.18564.
- [7] F. Lévy, I. Sheikin, B. Grenier, and A. D. Huxley. Magnetic Field-Induced Superconductivity in the Ferromagnet URhGe. *Science*, 309(5739):1343–1346, 2005. ISSN 0036-8075. doi:10.1126/science.1115498.
- [8] Atsushi Miyake, Yusei Shimizu, Yoshiki J Sato, Dexin Li, Ai Nakamura, Yoshiya Homma, Fuminori Honda, Jacques Flouquet, Masashi Tokunaga, and Dai Aoki. Metamagnetic Transition in Heavy Fermion Superconductor UTe₂ Letters. *Journal of the Physical Society of Japan*, 88:63706, 2019. doi:10.7566/jpsj.88.063706. URL <https://doi.org/10.7566/JPSJ.88.063706>.
- [9] Atsushi Miyake, Yusei Shimizu, Yoshiki J. Sato, Dexin Li, Ai Nakamura, Yoshiya Homma, Fuminori Honda, Jacques Flouquet, Masashi Tokunaga, and Dai Aoki. Enhancement and Discontinuity of Effective Mass through the First-Order Metamagnetic Transition in UTe₂. *Journal of the Physical Society of Japan*, 90(10):103702, 2021. ISSN 0031-9015. doi:10.7566/jpsj.90.103702.

- [10] K. A. Modic, Maja D. Bachmann, B. J. Ramshaw, F. Arnold, K. R. Shirer, Amelia Estry, J. B. Betts, Nirmal J. Ghimire, E. D. Bauer, Marcus Schmidt, Michael Baenitz, E. Svanidze, Ross D. McDonald, Arkady Shekhter, and Philip J.W. Moll. Resonant torsion magnetometry in anisotropic quantum materials. *Nature Communications* 2018 9:1, 9:1–8, 9 2018. doi:10.1038/s41467-018-06412-w. URL <https://www.nature.com/articles/s41467-018-06412-w>.
- [11] Sheng Ran, I-Lin Liu, Yun Suk Eo, Daniel J. Campbell, Paul M. Neves, Wesley T. Fuhrman, Shanta R. Saha, Christopher Eckberg, Hyunsoo Kim, David Graf, Fedor Balakirev, John Singleton, Johnpierre Paglione, and Nicholas P. Butch. Extreme magnetic field-boosted superconductivity. *Nature Physics* 2019 15:12, 15:1250–1254, 10 2019. doi:10.1038/s41567-019-0670-x. URL <https://www.nature.com/articles/s41567-019-0670-x>.
- [12] A. Shekhter, R. D. McDonald, B. J. Ramshaw, and K. A. Modic. Magnetotropic susceptibility. *Physical Review B*, 108(3): 035111, 2023. ISSN 2469-9950. doi:10.1103/physrevb.108.035111.
- [13] Z Wu, T I Weinberger, A J Hickey, D V Chichinadze, D Shaffer, A Cabala, H Chen, M Long, T J Brumm, W Xie, Y Lin, Y Skourski, Z Zengwei, D E Graf, V Sechovsky, G G Lonzarich, I M Valiska, F M Grosche, and A G Eaton. Quantum critical fluctuations generate intensely magnetic field-resilient superconductivity in UTe₂. *arXiv*, 2024. doi:10.48550/arxiv.2403.02535.
- [14] Z Wu, T I Weinberger, A J Hickey, D V Chichinadze, D Shaffer, A Cabala, H Chen, M Long, T J Brumm, W Xie, Y Lin, Y Skourski, Z Zhu, D E Graf, V Sechovsky, G G Lonzarich, M Valiska, F M Grosche, and A G Eaton. A quantum critical line bounds the high field metamagnetic transition surface in UTe. *arXiv*, 2024. doi:10.48550/arxiv.2403.02535v3.

Supplementary information for “Giant transverse magnetic susceptibility at the edge of re-entrant superconductivity in UTe_2 ”

I. CRYSTAL SYNTHESIS

Crystal was synthesized using the chemical vapor transport method, with iodine as the transport agent and a 5:9 starting ratio of U:Te. The sample was grown in a temperature gradient of 900/830°C for two weeks. Between measurements, the samples were stored in vacuum.

II. CRYSTAL AXES & ALIGNMENT

Accurate measurements of the magnetotropic susceptibility $k = \partial^2 F / \partial \theta^2$ are sensitive to the alignment of the crystallographic axes with respect to the external magnetic field. In order to identify the crystallographic axes, we performed x-ray scattering using a commercial Laue detector from Photonic Science. [Figure 1](#) shows the a - and b -axes of the orthorhombic structure of UTe_2 .

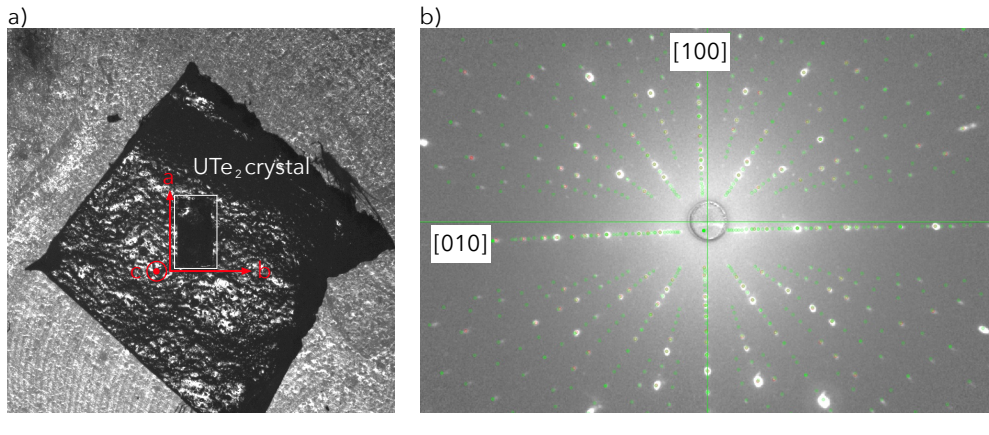


FIG. 1. **Laue diffraction on Sample #2** The crystal was mounted with the c -axis perpendicular to the surface of a scanning electron microscopy (SEM) stub. An example of the diffraction spectra showing the alignment of the a -axis and b -axis relative to the sample.

After identifying the a - and b -axis using the Laue, the axes were marked on the stub and were kept track of when cutting small pieces off for Sample #2 and Sample #3, and for cutting in the FIB chamber for sample #1.

III. SAMPLE PREPARATION

In highly-anisotropic materials, magnetotropic signal sizes vary substantially with magnetic field orientation. In order to achieve an appropriate signal size in the magnetotropic measurements for magnetic field rotated throughout these highly-anisotropic planes (i.e. to avoid breaking the cantilever), we need to prepare small samples. In total, we prepared 3 samples from 2 different bulk pieces (separate single crystals from the same batch). Two samples were cut by hand, and for one sample (Sample #1 used in the main text) we used the Helios G4 xenon plasma focused-ion beam (FIB). Use of the FIB allowed for better sample alignment. The overall trends in the high-field results, from both the ac - and bc -plane measurement, are consistent between all three samples, with slight differences due to misalignment and the high sensitivity of UTe_2 to field angle. Sample information is summarized in [Table I](#) below.

TABLE I. Summary of the samples measured and their relevant parameters

Sample	Bulk	Type	Volume [μm^3]	mol of U	k for 1 Hz [J/mol]
1	A	FIB'ed	72,914	1.36×10^{-9}	0.77
2	B	Hand cut	456,624	8.53×10^{-9}	0.54
3	B	Hand cut	568,620	1.06×10^{-8}	0.43

Once the crystal axes were identified with respect to the macroscopic crystal, the sample was mounted with the b -axis perpendicular to the surface of the sample holder and placed into the FIB chamber ([Figure 2](#)). Samples were cut from the bulk single crystal using small currents (4-15 nA) at 20 kV to minimize sample heating and surface damage.

After cutting and polishing the sides of the samples using the ion beam, the samples were left hanging from the bulk crystal by a $\sim 1 \times 1 \mu\text{m}^2$ bridge. Under an optical microscope, Sample #1 was manually disconnected from the bulk piece using an eyelash and a kapton needle. Before transferring the sample to the silicon microcantilever for measurements, a small drop of Apiezon L grease was placed on the lever to ensure that magnetic torque on the sample during measurements does not displace it. After measurements, we check that the placement of the sample on the lever remained intact.

Sample #2 and Sample #3 were cut using a razor blade from a different bulk sample than Sample #1. Before cutting the crystal, we used Laue to confirm the crystal axes. We then painted each face a different color in order to correlate the crystal axes in the cut piece with those from the Laue results.

For both measurement planes, the c -axis of the sample was mounted perpendicular to the surface of the lever and the a - or b -axis was mounted parallel to the long axis of the lever, depending upon the plane of anisotropy to be measured (ac - or bc -plane). After measurements in the first plane, the sample was rotated under an optical microscope by hand by $\sim 90^\circ$.

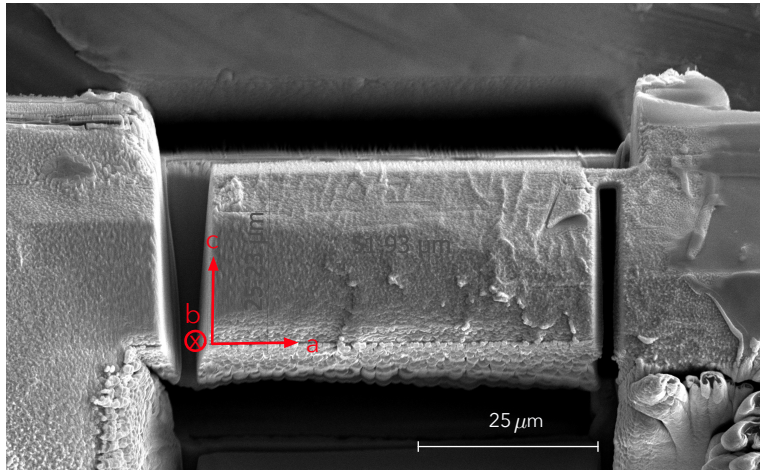


FIG. 2. FIB-ed UTe_2 Sample #1 The dimensions are $\sim 52 \times 66 \times 25 \mu\text{m}^3$.

IV. MAGNETOTROPIC MEASUREMENTS

We used the Nanosensors Akiyama-probe – a commercial silicon microcantilever developed for atomic force microscopy [1, 2]. The lever is connected to a quartz tuning fork that electrically drives and detects the resonance frequency of the coupled (fork + lever) oscillators. By operating at the fundamental bending mode of the lever, which ranges from ~ 35 to 40 kHz, we probe anisotropy in the plane of the principal axes that are in the plane of oscillation and field rotation [4].

The magnetotropic measurements were carried out at the National High Magnetic Field Laboratory (NHMFL) in Los Alamos National Laboratory, USA. The tuning fork with the cantilever attached was mounted onto a G10 substrate. The substrate is designed to ensure proper alignment and contact between the fork and the substrate. The G10 substrate is then attached to the stage of the rotator probe. The probe is then inserted into a vacuum-walled stainless steel fridge and the probe space is pumped down to 10^{-5} mbar. The fridge is inserted into a helium-4 cryostat. By introducing a small amount of exchange gas into the sample space, the sample reaches $T = 4$ K (note that atmospheric pressure in Los Alamos is substantially lower than at sea level and liquid helium is close to 4 K at these altitudes). In order to avoid the magnetic response of the superconductivity itself, a majority of our measurements were performed at 4 K. However, for a few measurements, we pumped on the bath of helium-4 to reach $T = 1.6$ K and measured below T_c (Figure 3).

A frequency scan is performed once the measurement temperature is stable to identify the resonant frequency. We drive the cantilever at its resonance frequency before the field pulse and then, just before discharging the capacitor bank to the magnet, a trigger signal is sent to stop the cantilever drive and the cantilever oscillates freely. Throughout the magnetic field pulse, the magnetotropic susceptibility leads to shifts in the oscillation frequency, and the raw data is collected with a digitizer for post-processing. The magnetic field versus time has a full-width at half maximum of ~ 10 ms. The total duration of the pulse, including its slow decay, is ~ 100 ms. By the end of the pulse, the amplitude of the resonant frequency, which is also consistently monitored, decays to about 50% of its drive value. With a resonance frequency of roughly 40 kHz, a single lever oscillation cycle occurs in $25 \mu\text{s}$. Several oscillations are analyzed over small time windows of 100 - $250 \mu\text{s}$ to find the resonance frequency, and the windows are stepped by $20 \mu\text{s}$ to generate

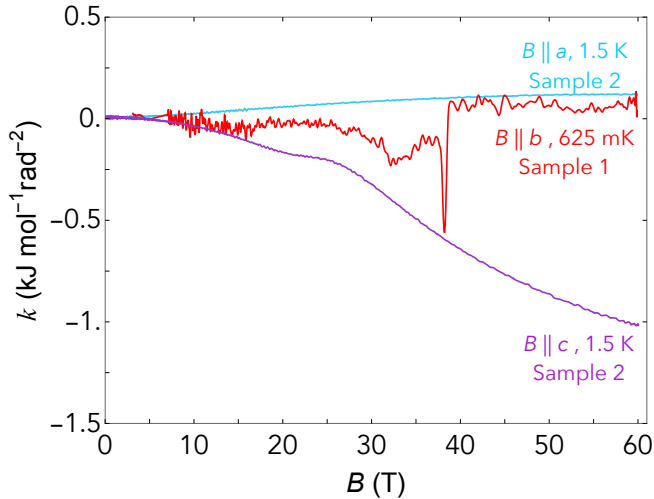


FIG. 3. **Magnetotropic measurements in the superconducting state** At temperatures below T_c (1.85 K in our samples), the magnetotropic susceptibility versus magnetic field for the three crystallographic directions. On Sample #1, k was measured for $B||b$ at $T = 625$ mK. The large increase in noise is due to the reduction in vibration damping because the ^4He bath is superfluid at these temperatures. The onset of the magnetotropic softening – small at this angle – is visible as a downturn near 25 T as a precursor to the metamagnetic transition near 35 T. The large magnetotropic softening near 20 T in Sample #2 at 1.5 K reproduces the main finding in the manuscript observed in the bc -plane for Sample #1. The blue curve shows k for $B||a$, also for Sample #2, which exhibits an essentially flat response up to 60 T – again consistent with Figure 2c in the manuscript.

each data point. The zero-field frequency is always remeasured between measurements taken at new field angles (*i.e.* after rotating the sample).

IV.1. Reproducibility

We performed high-field magnetotropic measurements on two different bulk crystals: Sample #1 was FIB'ed and Samples #2 and #3 were cut from a bulk piece using a razor blade. The data included in the main text was taken from Sample #1. We also acquired data in the ac - and bc -planes for Sample #2 and Sample #3. We find that the data taken across all samples is consistent; in particular, the large decrease in magnetotropic susceptibility, indicating a large increase in transverse susceptibility in the bc plane, is consistent between samples.

Figure 3 shows the magnetotropic susceptibility taken at temperatures below T_c for field aligned along each of the crystallographic directions in two different samples. The red curve shows data taken at the lowest temperature of 625 mK. The overall features observed in Figure 2 c&d at $T = 4$ K in the manuscript are reproduced here in Figure 3. The key consistencies are: i) the overall magnitude of the signal for all field configurations (*i.e.* a small response for $B||a$ and $B||b$ up to 60 T) ii) the onset of softening near 20 T and the metamagnetic transition near 35 T for $B||b$, and iii) the large softening that onsets near 20 T for $B||c$. This also demonstrates that the transverse softening persists down to low temperatures.

Figure 4 demonstrates that the main findings observed in the magnetotropic susceptibility in Sample #1 (a FIB'ed sample) of the manuscript are reproduced here for two different samples. In particular, we find 1) a large softening observed at ~ 20 T for a wide range of angles in both the ac - and bc -plane and 2) a critical endpoint to the line of first-order metamagnetic transitions in the bc -plane. In Sample #3, we observe that the softening onsets at a slightly lower field of ~ 10 T compared to ~ 20 T in Sample #1 in the manuscript. We also observe a large discontinuity in the middle of the field range over which the softening occurs for several angles near the c -axis, for measurements both in the ac - and bc -planes. This jump down followed by a peak in the magnetotropic susceptibility upon approaching 20 T is characteristic of a second-order phase transition, which was not observed in Sample #1. We attribute this difference to slight misalignments of the bc -plane on the lever for both samples; we believe in Sample #1, we precess around the phase transition observed in Sample #3. This is in agreement with the fact that the metamagnetic transition and the critical endpoint also occur at slightly different angles in both experiments. Alignment of our samples, which are only 100's of nanograms, is a technical challenge. As all features in UTe_2 are highly-anisotropic, one expects that slight misalignments may lead to variation in the positions of features observed with angle. Assuming $\approx 10^\circ$ offsets, our data are consistent with that of Lewin et al. [3].

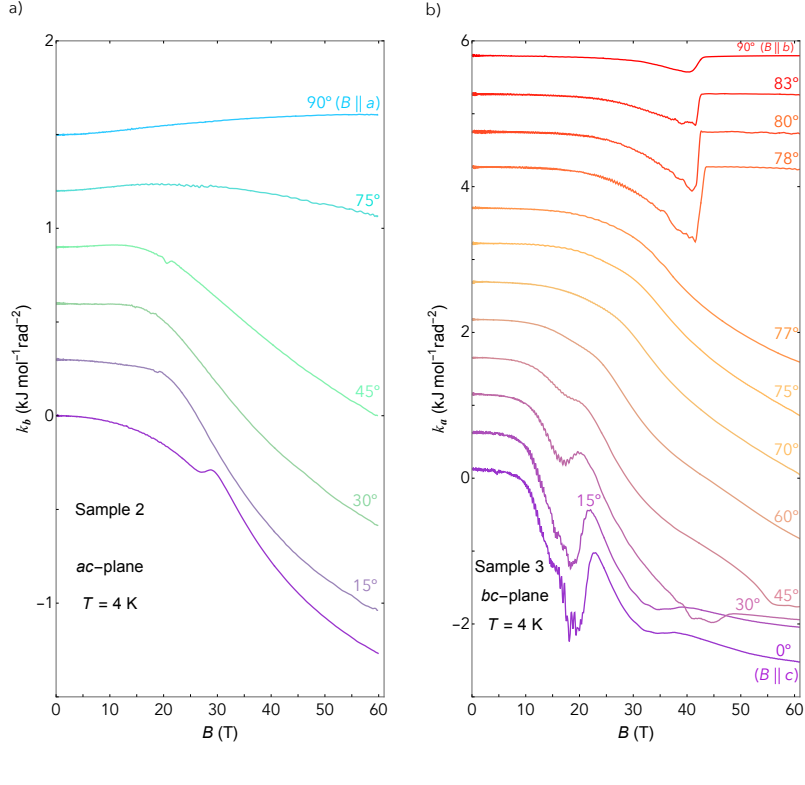


FIG. 4. **Magnetotropic susceptibility in the ac - and bc -planes** a) The ac -plane of Sample #2 was rotated with respect to field for several 60 T magnetic field pulses. A large decrease in the magnetotropic susceptibility is observed, similar in magnitude to that observed in Figure 2 of the main text. b) For rotation in the bc -plane, a large decrease in the magnetotropic susceptibility is again observed in a region consistent with the data shown in the main text. Between $\theta = 77^\circ$ and $\theta = 78^\circ$, the softening is cut off by the metamagnetic phase boundary that extends from $B||b$. The difference in B^* between this data and the data in the main text is due to a great degree of sample misalignment for this sample. However, the features as a function of angle are consistent with other studies if we assume an angle offset [3]. A large discontinuity indicating a possible second-order phase transition—possibly the B^* line from the second-order endpoint of the metamagnetic transition—is observed near 20 T in Sample #3.

V. CALIBRATION

In order to convert the measured frequency into the correct magnetotropic susceptibility units (J/mol/rad^2), we use the linear response regime $M_i = \chi_{ij}H_j$. Here, the frequency shift, which is directly proportional to the magnetotropic susceptibility, follows a characteristic field- and angle-dependence $k = (\chi_i - \chi_j)\cos 2\theta B^2$, where i, j describe the principal magnetic axes of the crystal in the plane of oscillation. Figure 5 shows the measured frequency shift vs B after subtracting their respective zero-field frequencies. After subtraction, a quadratic fit to the low-field (from ~ 1 -7 T) data gives the proportionality factor of the magnetic anisotropy.

A plot of the coefficient to the quadratic behavior in Figure 5a versus angle yields the anisotropy in the magnetic susceptibility, $\chi_i - \chi_j$ (Figure 5b). At $\theta = 0^\circ$, the amplitude is $\sim -0.47 \text{ Hz/T}^2$. The anisotropic susceptibility obtained through magnetic susceptibility measurements for field aligned along the a - and c -axes is $\chi_a - \chi_c = 0.36 \text{ J/T}^2/\text{mol}$ [5]. This can be equated with the amplitude of angle-dependent k measurements

$$0.47 \left[\frac{\text{Hz}}{\text{T}^2} \right] \rightarrow 0.36 \left[\frac{\text{J}}{\text{T}^2 \text{ mol}} \right] \quad (1)$$

Therefore, the conversion factor applied to the magnetotropic measurements for Sample #1 is $1 \text{ Hz} \rightarrow 0.77 \text{ J/mol/rad}^2$.

Because the anisotropy in the bc -plane at low fields is so small, the same calibration factor was applied to the bc -plane data for unit conversion. This is valid because we use the same sample on the same cantilever, and thus the calibration factor—related to the bending stiffness of the cantilever—is the same.

The magnetotropic susceptibility divided by magnetic field can be represented in units of magnetization. Based on the volume of the sample, the unit cell volume, and the fact that each (conventional) unit cell has 4 uranium atoms, we estimate 1.36×10^{-9} moles of uranium in Sample #1. With $\mu_B = 9.2 \times 10^{-24} \text{ J/T}$, this allows for conversion of the frequency shift into units of μ_B per U:

$$1 \left[\frac{\text{Hz}}{\text{T}} \right] \rightarrow 0.14 \left[\frac{\mu_B}{\text{U}} \right]. \quad (2)$$

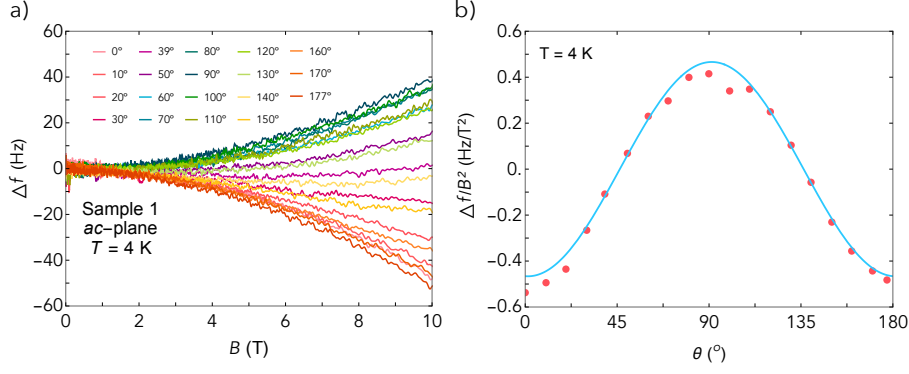


FIG. 5. **Magnetotropic susceptibility at low fields on Sample #1 in the ac -plane** a) At $T = 4$ K, the measured frequency shift after subtracting the zero-field frequency versus magnetic field up to 10 T at various field orientations. The frequency shift is proportional to the magnetotropic susceptibility, which has a quadratic field dependence at low fields due to a linear-in-field magnetization. b) The coefficient to the quadratic-in-field dependence of the magnetotropic susceptibility follows a $\cos^2\theta$ dependence and is proportional to the anisotropic magnetic susceptibility in the plane of vibration ($\chi_i - \chi_j$).

- [1] Terunobu Akiyama, Nicolaas F. de Rooij, Urs Stauffer, Manfred Detterbeck, Dominik Braendlin, Simon Waldmeier, and Martin Scheidiger. Implementation and characterization of a quartz tuning fork based probe consisted of discrete resonators for dynamic mode atomic force microscopy. *Review of Scientific Instruments*, 81(6):063706, 2010. ISSN 0034-6748. doi:10.1063/1.3455219.
- [2] Wilton J M Kort-Kamp, Ryan A Murdick, Han Htoon, and Andrew C Jones. Utilization of coupled eigenmodes in Akiyama atomic force microscopy probes for bimodal multifrequency sensing. *Nanotechnology*, 33(45):455501, 2022. ISSN 0957-4484. doi:10.1088/1361-6528/ac8232.
- [3] Sylvia K Lewin, Peter Czajka, Corey E Frank, Gicela Saucedo Salas, Hyeok Yoon, Yun Suk Eo, Johnpierre Paglione, Andriy H Nevidomskyy, John Singleton, and Nicholas P Butch. High-Field Superconducting Halo in UTe₂. *arXiv*, 2024. doi:10.48550/arxiv.2402.18564.
- [4] K. A. Modic, Maja D. Bachmann, B. J. Ramshaw, F. Arnold, K. R. Shirer, Amelia Estry, J. B. Betts, Nirmal J. Ghimire, E. D. Bauer, Marcus Schmidt, Michael Baenitz, E. Svanidze, Ross D. McDonald, Arkady Shekhter, and Philip J.W. Moll. Resonant torsion magnetometry in anisotropic quantum materials. *Nature Communications* 2018 9:1, 9:1–8, 9 2018. doi:10.1038/s41467-018-06412-w. URL <https://www.nature.com/articles/s41467-018-06412-w>.
- [5] Priscila F. S. Rosa, Ashley Weiland, Shannon S. Fender, Brian L. Scott, Filip Ronning, Joe D. Thompson, Eric D. Bauer, and Sean M. Thomas. Single thermodynamic transition at 2 K in superconducting UTe₂ single crystals. *Communications Materials*, 3(1):33, 2022. doi:10.1038/s43246-022-00254-2.